MATHEMATICAL MODELING AND COMPUTING, Vol. 8, No. 4, pp. 807–820 (2021)

Numerical exploration of mixed convection heat transfer features within a copper-water nanofluidic medium occupied a square geometrical cavity

Zaydan M., Wakif A., Essaghir E., Sehaqui R.

Laboratory of Mechanics, Faculty of Sciences Ain-Chock, University Hassan II Casablanca, Morocco

(Received 23 May 2021; Accepted 7 June 2021)

The phenomenon of mixed convection heat transfer in a homogeneous mixture is deliberated thoroughly in this study for cooper-water nanofluids flowing inside a lid-driven square cavity. By adopting the Oberbeck–Boussinesq approximation and using the single-phase nanofluid model, the governing partial differential equations modeling the present flow are stated mathematically based on the Navier–Stokes and thermal balance formulations, where the important features of the scrutinized medium are presumed to remain constant at the cold temperature. Note here that the density quantity in the buoyancy body force is a linear temperature-dependent function. The characteristic quantities are computed realistically via the commonly used phenomenological laws and the more accurate experimental correlations. A feasible non-dimensionalization procedure has been employed to derive the dimensionless conservation equations. The resulting nonlinear differential equations are solved numerically for realistic boundary conditions by employing the fourth-order compact finite-difference method (FOCFDM). After performing extensive validations with the previously published findings, the dynamical and thermal features of the studied convective nanofluid flow are revealed to be in good agreement for sundry values of the involved physical parameters. Besides, the present numerical outcomes are discussed graphically and tabularly with the help of streamlines, isotherms, velocity fields, temperature distributions, and local heat transfer rate profiles.

Keywords: *nanofluid, mixed convection, square cavity, numerical simulation.*

2010 MSC: 35Q35, 37N10, 76E06, 65M06, 80A20 **DOI:** 10.23939/mmc2021.04.807

1. Introduction

Heat transfer enhancement issue in nanofluid-filled enclosures via the mixed-convection process has provided a vast scope for scientific research [1–4] due to its tremendous engineering and energy uses in everyday life and many field of industry (e.g., cooling equipment, solar collectors, chemical processing industries, float glass production, and drying technologies). In such a heat transfer occurrence, the laminar convective flows of nanofluids can be described mathematically by a system of classical [5–12] fractional [13,14] partial differential equations, which cannot be treated analytically or semi-analytically because of its higher nonlinearity and coupling equations. This is why several researchers [15–18] conducted similar problems numerically by applying powerful computational procedures, like the finite element method (FEM), finite volume method (FVM), and lattice Boltzmann method (LBM).

Energetically, the conventional cooling fluids (e.g., water, methanol, and ethylene glycol) exhibit remarkable limitations in terms of thermal energy storage and heat transfer efficiency. So, it is recommended to insert nano-sized solid particles of higher conductivity to improve the thermal features of the usual fluids [19, 20]. Various types of solid nanomaterials can be incorporated in the base fluids, such as metals, metal oxides, and non-metals. In this context, Tiwari and Das [21] evaluated numerically the heat transfer enhancement within the mixed convection flows within a square cavity filled by the copper-water. They conclude that the occurred pattern formation and the heat transfer rate were greatly influenced by the higher estimation of the mixed convention parameter and by the sense of the vertical moving walls. Several explorations have been reported in the literature for convective nanofluid flows [22–26]. For example, Rana and Bhargava [27] examined numerically the heat transfer enhancement in steady mixed convection nanofluid flow over a vertical plate in the presence of heat source/sink. In this scrutinization, it was shown that the silver nanoparticles can improve the cooling performance than the other used chemical species. Similarly, Zaraki et al. [28] adopted the non-homogeneous model of Buongiorno [29] to perform a theoretical analysis on the heat and mass transfer of the boundary layer nanofluid flows by analyzing the effects of size/shape/type of nanoparticles, type of base fluids, and working temperature. In a non-planar geometric configuration, Mebarek–Oudina [30] implemented an advanced FVM code to reveal the effect of different base fluids on the thermo-hydrodynamic characteristics of titania-based nanofluids in a cylindrical annulus with a discrete heat source. Besides, Wakif et al. [31–34] deliberated thoroughly the impacts of the haphazard motion of solid nanoparticles and their thermo-migration on the thermal appearances of mixtures at a nanometric scale.

Motivating by the above-discussed research works and the valuable applications of nanofluids, the present numerical scrutinization has been carried out to disclose the mixed convection heat transfer features in a two-sided lid-driven square cavity filled by copper-water nanofluids, in the case where the left cold wall is moving upwards and the right hot wall is moving downwards. The prime novelty of this study is to combine known phenomenological laws along with accurate experimental correlations in the proposed single-phase nanofluid model to generate realistic physical results via the fourth-order compact finite-difference method (FOCFDM).

2. Mathematical formulation

As sketched in Fig. 1, the problem of incompressible laminar flow of water-based nanofluid containing copper nanomaterials of spherical shape inside a two-dimensional square cavity of length L is simulated appropriately with the help of Cartesian coordinates. Thermally, the right wall is heated isothermally at a constant temperature T_H, whereas the temperature of the left side-wall is kept unchanged at the temperature $T_C = 300\,\mathrm{K}$ $(< T_H)$. Dynamically, the studied mixed convective nanofluid flow is driven by the uniform motion of the vertical walls $\tilde{x} = 0$ and $\tilde{x} = L$, their velocities are expressed respectively as $\tilde{v}(\tilde{x} = 0, \tilde{y}, \tilde{t}) = V_0$ and $\tilde{v}(\tilde{x} = L, \tilde{y}, \tilde{t}) = -V_0$. On the other hand, the horizontal walls are selected to be immobile and insulted. By adopting the linear form of the Oberbeck–Boussinesq approximation along with the single-phase nanofluid model [21], the nonlinear partial differential equations describing the present nanofluid flow problem are written as [35, 36]:

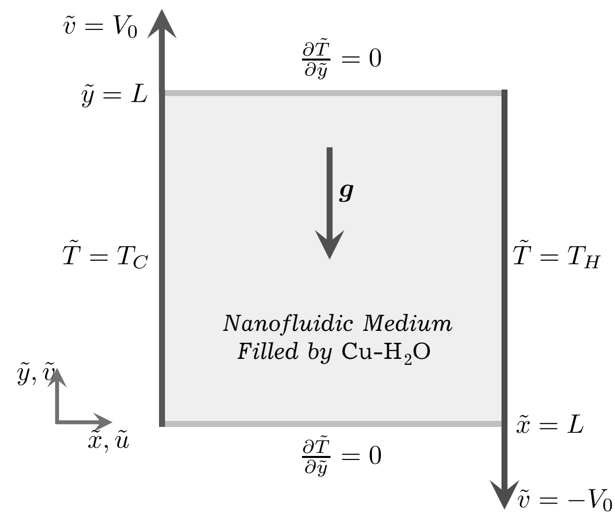

Fig. 1. Geometrical configuration of the present convective nanofluid flow problem.

$$\frac{\partial \tilde{u}}{\partial \tilde{x}} + \frac{\partial \tilde{v}}{\partial \tilde{y}} = 0, \tag{1}$$

$$\rho_{nf} \left(\frac{\partial \tilde{u}}{\partial \tilde{t}} + \tilde{u} \frac{\partial \tilde{u}}{\partial \tilde{x}} + \tilde{v} \frac{\partial \tilde{u}}{\partial \tilde{y}} \right) = -\frac{\partial \tilde{p}}{\partial \tilde{x}} + \mu_{nf} \left(\frac{\partial^2 \tilde{u}}{\partial \tilde{x}^2} + \frac{\partial^2 \tilde{u}}{\partial \tilde{y}^2} \right), \tag{2}$$

$$\rho_{nf}\left(\frac{\partial\tilde{v}}{\partial\tilde{t}}+\tilde{u}\frac{\partial\tilde{v}}{\partial\tilde{x}}+\tilde{v}\frac{\partial\tilde{v}}{\partial\tilde{y}}\right)=-\frac{\partial\tilde{P}}{\partial\tilde{y}}+\mu_{nf}\left(\frac{\partial^2\tilde{v}}{\partial\tilde{x}^2}+\frac{\partial^2\tilde{v}}{\partial\tilde{y}^2}\right)+(\rho\beta)_{nf}g\left(\tilde{T}-T_C\right), \tag{3}$$

$$(\rho C_p)_{nf}\left(\frac{\partial\tilde{T}}{\partial\tilde{t}}+\tilde{u}\frac{\partial\tilde{T}}{\partial\tilde{x}}+\tilde{v}\frac{\partial\tilde{T}}{\partial\tilde{y}}\right)=k_{nf}\left(\frac{\partial^2\tilde{T}}{\partial\tilde{x}^2}+\frac{\partial^2\tilde{T}}{\partial\tilde{y}^2}\right). \tag{4}$$

Here, $\tilde{p}$ is the pressure and $\tilde{P}$ is the modified pressure, where $\tilde{P}=\tilde{p}+\rho_{nf}g\tilde{y}$.

Those conservative equations are governed realistically by the following initial and boundary conditions:

$$\begin{cases}\tilde{u}\left(\tilde{x},\tilde{y},\tilde{t}=0\right)=0, & \tilde{u}\left(\tilde{x}=0,L,\tilde{y},\tilde{t}\right)=0, \quad \tilde{u}\left(\tilde{x},\tilde{y}=0,L,\tilde{t}\right)=0,\\ \tilde{v}\left(\tilde{x},\tilde{y},\tilde{t}=0\right)=0, & \tilde{v}\left(\tilde{x}=0,\tilde{y},\tilde{t}\right)=V_0, \quad \tilde{v}\left(\tilde{x}=L,\tilde{y},\tilde{t}\right)=-V_0, \quad \tilde{v}\left(\tilde{x},\tilde{y}=0,L,\tilde{t}\right)=0,\\ \tilde{T}\left(\tilde{x},\tilde{y},\tilde{t}=0\right)=T_C, & \tilde{T}\left(\tilde{x}=0,\tilde{y},\tilde{t}\right)=T_C, \quad \tilde{T}\left(\tilde{x}=L,\tilde{y},\tilde{t}\right)=T_H, \quad \left(\partial\tilde{T}/\partial\tilde{y}\right)_{\left(\tilde{x},\tilde{y}=0,L,\tilde{t}\right)}=0.\end{cases} \tag{5}$$

Besides, the thermophysical properties of copper-water nanofluids ρ_{nf}, μ_{nf}, $(\rho\beta)_{nf}$, $(\rho C_p)_{nf}$, and k_{nf} are formulated explicitly as functions of the nanoparticles volume fraction χ and other characteristics by the following expressions [37–43]:

$$\begin{cases}\rho_{nf}=\rho_{np}\chi+(1-\chi)\,\rho_f,\\ \mu_{nf}=\dfrac{\mu_f}{1-34.87\left(\frac{d_{np}}{d_f}\right)^{-0.3}\chi^{1.03}},\\ (\rho\beta)_{nf}=(\rho\beta)_{np}\chi+(\rho\beta)_f\,(1-\chi)\,,\\ (\rho C_P)_{nf}=(\rho C_P)_{np}\chi+(\rho C_P)_f\,(1-\chi)\,,\\ k_{nf}=\left[1+4.4\,\mathrm{Re}_B^{0.4}\,\mathrm{Pr}^{0.66}\left(\frac{T_C}{T_{Fr}}\right)^{10}\left(\frac{k_{np}}{k_f}\right)^{0.03}\chi^{0.66}\right]k_f,\\ \text{where }\ \mathrm{Pr}=\frac{\mu_f(\rho C_P)_f}{\rho_f k_f}\ \text{ and }\ \mathrm{Re}_B=\frac{2\rho_f k_B T_C}{\pi\,\mu_f^2\,d_{np}}.\end{cases} \tag{6}$$

In Eq. (5), the subscripts nf, f, and np are incorporated to indicate the nanofluid, the base fluid, and the solid nanoparticles, respectively. Moreover, the pertinent thermophysical properties of the nanofluid constituents are summarized clearly in Table 1. Furthermore, the physical meanings of all pertinent variables, quantities, and parameters are summarized and defined in the nomenclature tables.

Table 1. Thermophysical properties of the nanofluid constituents [33,44].

Thermophysical properties	Base fluid Water (H_2O)	Solid nanoparticles Copper (Cu)
d_{np} (nm)	0.385	30 – 60
ρ ($\mathrm{Kg\,m^{-3}}$)	997.1	8933
C_p ($\mathrm{J\ Kg^{-1}\ K^{-1}}$)	4179	385
k ($\mathrm{W\ m^{-1}\ K^{-1}}$)	0.613	401
β ($\times 10^{-4}\mathrm{K^{-1}}$)	2.1	0.167
μ (Pa s)	89×10^{-5}	—

To obtain the dimensionless conservation equations, the following dimensionless variables are introduced into the aforestated mathematical formulation:

$$x=\frac{\tilde{x}}{L},\quad y=\frac{\tilde{y}}{L},\quad t=\left(\frac{V_0}{L}\right)\tilde{t},\quad U=\frac{\tilde{u}}{V_0},\quad V=\frac{\tilde{v}}{V_0},\quad P=\frac{1}{\rho_f V_0^2}\tilde{P},\quad T=\frac{\tilde{T}-T_C}{T_H-T_C}. \tag{7}$$

Accordingly, Eqs. (1)–(4) are altered to:

$$\frac{\partial U}{\partial x}+\frac{\partial V}{\partial y}=0, \tag{8}$$

$$\frac{\partial U}{\partial t}+U\frac{\partial U}{\partial x}+V\frac{\partial U}{\partial y}=-\frac{\partial P}{\partial x}+\frac{\mu_r}{\rho_r\,\mathrm{Re}_w}\left(\frac{\partial^2 U}{\partial x^2}+\frac{\partial^2 U}{\partial y^2}\right), \tag{9}$$

$$\frac{\partial V}{\partial t}+U\frac{\partial V}{\partial x}+V\frac{\partial V}{\partial y}=-\frac{\partial P}{\partial y}+\frac{\mu_r}{\rho_r\,\mathrm{Re}_w}\left(\frac{\partial^2 V}{\partial x^2}+\frac{\partial^2 V}{\partial y^2}\right)+\frac{(\rho\beta)_r\mathrm{Ri}}{\rho_r}T, \tag{10}$$

$$\frac{\partial T}{\partial t}+U\frac{\partial T}{\partial x}+V\frac{\partial T}{\partial y}=\frac{k_r}{(\rho C_P)_r\,\mathrm{Pr}\,\mathrm{Re}_w}\left(\frac{\partial^2 T}{\partial x^2}+\frac{\partial^2 T}{\partial y^2}\right). \tag{11}$$

In this stage, the initial and boundary conditions given by Eq. (5) are simplified as:

$$\begin{cases} U(x,y,t=0)=0, \quad U(x=0,1,y,t)=0, \quad U(x,y=0,1,t)=0, \\ V(x,y,t=0)=0, \quad V(x=0,y,t)=1, \quad V(x=1,y,t)=-1, \quad V(x,y=0,1,t)=0, \\ T(x,y,t=0)=0, \quad T(x=0,y,t)=0, \quad T(x=1,y,t)=1, \quad (\partial T/\partial y)_{(x,y=0,1,t)}=0. \end{cases} \tag{12}$$

For more clarification, the dimensionless physical parameters and quantities appeared above are expressed as follows:

$$\begin{cases} \mathrm{Ri}=\dfrac{Gr}{\mathrm{Re}_w^2}, \quad Gr=\dfrac{(\rho\beta)_f\,(T_H-T_C)\,gL^3}{\nu_f\mu_f}, \quad \mathrm{Re}_w=\dfrac{V_0L}{\nu_f}, \\ \rho_r=\dfrac{\rho_{nf}}{\rho_f}, \quad \mu_r=\dfrac{\mu_{nf}}{\mu_f}, \quad (\rho\beta)_r=\dfrac{(\rho\beta)_{nf}}{(\rho\beta)_f}, \quad (\rho C_P)_r=\dfrac{(\rho C_P)_{nf}}{(\rho C_P)_f}, \quad k_r=\dfrac{k_{nf}}{k_f}. \end{cases} \tag{13}$$

Herein, the stream function ψ and the vorticity ω are defined as:

$$\begin{cases} U=\dfrac{\partial\psi}{\partial y}, \\ V=-\dfrac{\partial\psi}{\partial x}, \\ \omega=\dfrac{\partial V}{\partial x}-\dfrac{\partial U}{\partial y}. \end{cases} \tag{14}$$

By incorporating the above expressions into Eqs. (8)–(11), the ψ–ω formulation of the present nanofluid flow problem is stated as follows:

$$\frac{\partial^2\psi}{\partial x^2}+\frac{\partial^2\psi}{\partial y^2}=-\omega, \tag{15}$$

$$\frac{\partial\omega}{\partial t}+\left(\frac{\partial\psi}{\partial y}\right)\left(\frac{\partial\omega}{\partial x}\right)-\left(\frac{\partial\psi}{\partial x}\right)\left(\frac{\partial\omega}{\partial y}\right)=\frac{\mu_r}{\rho_r\,\mathrm{Re}_w}\left(\frac{\partial^2\omega}{\partial x^2}+\frac{\partial^2\omega}{\partial y^2}\right)+\frac{(\rho\beta)_r\mathrm{Ri}}{\rho_r}\frac{\partial T}{\partial x}, \tag{16}$$

$$\frac{\partial T}{\partial t}+\left(\frac{\partial\psi}{\partial y}\right)\left(\frac{\partial T}{\partial x}\right)-\left(\frac{\partial\psi}{\partial x}\right)\left(\frac{\partial T}{\partial y}\right)=\frac{k_r}{(\rho C_P)_r\,\mathrm{Pr}\,\mathrm{Re}_w}\left(\frac{\partial^2 T}{\partial x^2}+\frac{\partial^2 T}{\partial y^2}\right). \tag{17}$$

Generally, Eqs. (16) and (17) can be rewritten as:

$$\frac{\partial\Gamma}{\partial t}+\left(\frac{\partial\psi}{\partial y}\right)\left(\frac{\partial\Gamma}{\partial x}\right)-\left(\frac{\partial\psi}{\partial x}\right)\left(\frac{\partial\Gamma}{\partial y}\right)=\varepsilon\left(\frac{\partial^2\Gamma}{\partial x^2}+\frac{\partial^2\Gamma}{\partial y^2}\right)+\eta\left(\frac{\partial T}{\partial x}\right), \tag{18}$$

in which

$$\begin{cases} (\varepsilon,\eta)_{\Gamma=\omega}=\left(\dfrac{\mu_r}{\rho_r\,\mathrm{Re}_w},\dfrac{(\rho\beta)_r\mathrm{Ri}}{\rho_r}\right), \\ (\varepsilon,\eta)_{\Gamma=T}=\left(\dfrac{k_r}{(\rho C_P)_r\,\mathrm{Pr}\,\mathrm{Re}_w},0\right), \\ \psi(x=0,1,y,t)=0, \\ \psi(x,y=0,1,t)=0. \end{cases} \tag{19}$$

3. Solution methodology

By employing the fourth-order compact finite-difference schemes in the (x, y)-directions [45], the first and second derivatives of a function $\Phi(x, y, t)$ are approximated by:

$$\begin{cases} \dfrac{\partial \Phi}{\partial x} = \Phi_x - \left(\dfrac{\Delta x^2}{6}\right)\left(\dfrac{\partial^3 \Phi}{\partial x^3}\right) + \mathrm{O}\left(\Delta x^4\right), \\ \dfrac{\partial \Phi}{\partial y} = \Phi_y - \left(\dfrac{\Delta y^2}{6}\right)\left(\dfrac{\partial^3 \Phi}{\partial y^3}\right) + \mathrm{O}\left(\Delta y^4\right), \\ \dfrac{\partial^2 \Phi}{\partial x^2} = \Phi_{xx} - \left(\dfrac{\Delta x^2}{12}\right)\left(\dfrac{\partial^4 \Phi}{\partial x^4}\right) + \mathrm{O}\left(\Delta x^4\right), \\ \dfrac{\partial^2 \Phi}{\partial y^2} = \Phi_{yy} - \left(\dfrac{\Delta y^2}{12}\right)\left(\dfrac{\partial^4 \Phi}{\partial y^4}\right) + \mathrm{O}\left(\Delta y^4\right). \end{cases} \tag{20}$$

Under the above considerations, the steady-state of Eqs. (15) and (18) leads to the following approximations:

$$\psi_{xx} + \psi_{yy} - \left(\frac{\Delta x^2}{12}\right)\left(\frac{\partial^4 \psi}{\partial x^4}\right) - \left(\frac{\Delta y^2}{12}\right)\left(\frac{\partial^4 \psi}{\partial y^4}\right) + \mathrm{O}\left(\Delta x^4, \Delta y^4\right) = -\omega. \tag{21}$$

$$\begin{aligned} \varepsilon \Gamma_{xx} + \varepsilon \Gamma_{yy} - \varepsilon \left(\frac{\Delta x^2}{12}\right)\left(\frac{\partial^4 \Gamma}{\partial x^4}\right) - \varepsilon \left(\frac{\Delta y^2}{12}\right)\left(\frac{\partial^4 \Gamma}{\partial y^4}\right) + \mathrm{O}\left(\Delta x^4, \Delta y^4\right) = \psi_y \Gamma_x \\ - \psi_x \Gamma_y - \left(\frac{\Delta y^2}{6}\right)\Gamma_x \left(\frac{\partial^3 \psi}{\partial y^3}\right) - \left(\frac{\Delta x^2}{6}\right)\psi_y \left(\frac{\partial^3 \Gamma}{\partial x^3}\right) + \left(\frac{\Delta x^2}{6}\right)\Gamma_y \left(\frac{\partial^3 \psi}{\partial x^3}\right) \\ + \left(\frac{\Delta y^2}{6}\right)\psi_x \left(\frac{\partial^3 \Gamma}{\partial y^3}\right) - \eta T_x + \eta \left(\frac{\Delta x^2}{6}\right)\left(\frac{\partial^3 T}{\partial x^3}\right) + \mathrm{O}\left(\Delta x^4, \Delta x^2 \Delta y^2, \Delta y^4\right). \end{aligned} \tag{22}$$

Similarly, we have from Eqs. (15) and (18):

$$\frac{\partial^3 \psi}{\partial x^3} = -\frac{\partial \omega}{\partial x} - \frac{\partial^3 \psi}{\partial x \partial y^2}, \tag{23}$$

$$\frac{\partial^4 \psi}{\partial x^4} = -\frac{\partial^2 \omega}{\partial x^2} - \frac{\partial^4 \psi}{\partial x^2 \partial y^2}, \tag{24}$$

$$\frac{\partial^3 \psi}{\partial y^3} = -\frac{\partial \omega}{\partial y} - \frac{\partial^3 \psi}{\partial y \partial x^2}, \tag{25}$$

$$\frac{\partial^4 \psi}{\partial y^4} = -\frac{\partial^2 \omega}{\partial y^2} - \frac{\partial^4 \psi}{\partial y^2 \partial x^2}, \tag{26}$$

$$\begin{aligned} \frac{\partial^3 \Gamma}{\partial x^3} = \frac{1}{\varepsilon}\left(\frac{\partial^2 \psi}{\partial x \partial y}\right)\left(\frac{\partial \Gamma}{\partial x}\right) + \frac{1}{\varepsilon}\left(\frac{\partial \psi}{\partial y}\right)\left(\frac{\partial^2 \Gamma}{\partial x^2}\right) - \frac{1}{\varepsilon}\left(\frac{\partial^2 \psi}{\partial x^2}\right)\left(\frac{\partial \Gamma}{\partial y}\right) - \frac{1}{\varepsilon}\left(\frac{\partial \psi}{\partial x}\right)\left(\frac{\partial^2 \Gamma}{\partial x \partial y}\right) \\ - \frac{\eta}{\varepsilon}\left(\frac{\partial^2 T}{\partial x^2}\right) - \left(\frac{\partial^3 \Gamma}{\partial x \partial y^2}\right), \end{aligned} \tag{27}$$

$$\begin{aligned} \frac{\partial^4 \Gamma}{\partial x^4} = \frac{1}{\varepsilon}\left(\frac{\partial^3 \psi}{\partial x^2 \partial y}\right)\left(\frac{\partial \Gamma}{\partial x}\right) + \frac{1}{\varepsilon}\left(\frac{\partial^2 \psi}{\partial x \partial y}\right)\left(\frac{\partial^2 \Gamma}{\partial x^2}\right) + \frac{1}{\varepsilon}\left(\frac{\partial^2 \psi}{\partial x \partial y}\right)\left(\frac{\partial^2 \Gamma}{\partial x^2}\right) \\ + \frac{1}{\varepsilon}\left(\frac{\partial \psi}{\partial y}\right)\left(\frac{\partial^3 \Gamma}{\partial x^3}\right) - \frac{1}{\varepsilon}\left(\frac{\partial^3 \psi}{\partial x^3}\right)\left(\frac{\partial \Gamma}{\partial y}\right) - \frac{1}{\varepsilon}\left(\frac{\partial^2 \psi}{\partial x^2}\right)\left(\frac{\partial^2 \Gamma}{\partial x \partial y}\right) \\ - \frac{1}{\varepsilon}\left(\frac{\partial^2 \psi}{\partial x^2}\right)\left(\frac{\partial^2 \Gamma}{\partial x \partial y}\right) - \frac{1}{\varepsilon}\left(\frac{\partial \psi}{\partial x}\right)\left(\frac{\partial^3 \Gamma}{\partial x^2 \partial y}\right) - \frac{\eta}{\varepsilon}\left(\frac{\partial^3 T}{\partial x^3}\right) - \left(\frac{\partial^4 \Gamma}{\partial x^2 \partial \mathrm{y}^2}\right). \end{aligned} \tag{28}$$

After many simplifications and rearrangements, we get finally the following fourth-order compact formulation (FOCF):

$$\psi_{xx}+\psi_{yy}=-\omega+A, \tag{29}$$

$$\varepsilon\left(1+B\right)\Gamma_{xx}+\varepsilon\left(1+C\right)\Gamma_{yy}=\left(\psi_y+D\right)\Gamma_x-\left(\psi_x+E\right)\Gamma_y-\left(\frac{\eta}{\Upsilon_1}\right)T_x+F, \tag{30}$$

in which

$$A=-\left(\frac{\Delta x^2}{12}\right)\omega_{xx}-\left(\frac{\Delta y^2}{12}\right)\omega_{yy}-\Delta_{xy}\psi_{xxyy}, \tag{31}$$

$$B=-\frac{1}{\varepsilon}\left(\frac{\Delta x^2}{6}\right)\psi_{xy}+\frac{1}{\varepsilon^2}\left(\frac{\Delta x^2}{12}\right)\psi_y\psi_y, \tag{32}$$

$$C=\frac{1}{\varepsilon}\left(\frac{\Delta y^2}{6}\right)\psi_{xy}+\frac{1}{\varepsilon^2}\left(\frac{\Delta y^2}{12}\right)\psi_x\psi_x, \tag{33}$$

$$D=\Delta_{xy}\psi_{xxy}-\frac{1}{\varepsilon}\left(\frac{\Delta x^2}{12}\right)\psi_y\psi_{xy}+\frac{1}{\varepsilon}\left(\frac{\Delta y^2}{12}\right)\psi_x\psi_{yy}, \tag{34}$$

$$E=\Delta_{xy}\psi_{xyy}-\frac{1}{\varepsilon}\left(\frac{\Delta x^2}{12}\right)\psi_y\psi_{xx}+\frac{1}{\varepsilon}\left(\frac{\Delta y^2}{12}\right)\psi_x\psi_{xy}, \tag{35}$$

$$\begin{aligned}F=\Delta_{xy}\psi_y\Gamma_{xyy}-\Delta_{xy}\psi_x\Gamma_{xxy}-\frac{1}{\varepsilon}\left(\frac{\Delta x^2}{6}\right)\psi_{xx}\Gamma_{xy}+\left(\frac{\Delta y^2}{6}\right)\psi_{yy}\Gamma_{xy}+\frac{\Delta_{xy}}{\varepsilon}\psi_x\psi_y\Gamma_{xy}\\-\frac{1}{\varepsilon}\left(\frac{\Delta x^2}{12}-\frac{\Delta y^2}{12}\right)\Gamma_x\Gamma_y-\Delta_{xy}\Gamma_{xxyy}+\eta G,\end{aligned} \tag{36}$$

$$\begin{aligned}G=\frac{\Upsilon_2}{\Upsilon_1}\left(\frac{\Delta x^2}{12}\right)\psi_{xy}T_x+\left(\frac{\Upsilon_2}{\Upsilon_1}+\frac{1}{{\Upsilon_1}^2}\right)\left(\frac{\Delta x^2}{12}\right)\psi_yT_{xx}-\left(\frac{\Upsilon_2}{\Upsilon_1}\right)\left(\frac{\Delta x^2}{12}\right)\psi_{xx}T_y\\-\left(\frac{\Upsilon_2}{\Upsilon_1}\frac{\Delta x^2}{12}+\frac{1}{\Upsilon_1^2}\frac{\Delta y^2}{12}\right)\psi_xT_{xy}-\frac{\Delta_{xy}}{\Upsilon_1}T_{xyy},\end{aligned} \tag{37}$$

$$\Delta_{xy}=\frac{\Delta x^2}{12}+\frac{\Delta y^2}{12} \tag{38}$$

$$\Upsilon_1=\frac{\mu_r}{\rho_r\,\mathrm{Re}_w}, \tag{39}$$

$$\Upsilon_2=\frac{k_r}{\left(\rho C_P\right)_r\mathrm{Pr}\,\mathrm{Re}_w}. \tag{40}$$

It bears noting here that the resulting differential system along with their associated boundary conditions can be integrated numerically via the alternating directions implicit iteration as explained by Peaceman and Rachford [46]. In this framework, the system of Eqs. (15) and (18) is rewritten as follow:

$$\psi^n+\Delta t\left(\frac{\partial^2\psi}{\partial x^2}\right)^{n+1}+\Delta t\left(\frac{\partial^2\psi}{\partial y^2}\right)^{n+1}=-\Delta t\,\omega^n+\psi^{n+1}, \tag{41}$$

$$\begin{aligned}\Gamma^{n+1}+\Delta t\left(\frac{\partial\psi}{\partial y}\right)^n\left(\frac{\partial\Gamma}{\partial x}\right)^{n+1}-\Delta t\left(\frac{\partial\psi}{\partial x}\right)^n\left(\frac{\partial\Gamma}{\partial y}\right)^{n+1}\\=\varepsilon\Delta t\left[\left(\frac{\partial^2\Gamma}{\partial x^2}\right)^{n+1}+\left(\frac{\partial^2\Gamma}{\partial y^2}\right)^{n+1}\right]+\eta\Delta t\left(\frac{\partial T}{\partial x}\right)^{n+1}+\Gamma^n.\end{aligned} \tag{42}$$

According to Erturk and Gökcöl [47], the solution of Eqs. (41) and (42) converges always to a stationary regime. In this respect, different residual errors can be evaluated:

$$\left(\mathrm{Re}\,s_1\right)_\psi=\max\left(\left|\frac{\psi_{i-1,j}^{n+1}-2\psi_{i,j}^{n+1}+\psi_{i+1,j}^{n+1}}{\Delta x^2}+\frac{\psi_{i,j-1}^{n+1}-2\psi_{i,j}^{n+1}+\psi_{i,j+1}^{n+1}}{\Delta y^2}+\omega_{i,j}^{n+1}-A_{i,j}^{n+1}\right|\right), \tag{43}$$

$$(\mathrm{Re}\,s_1)_\Gamma = \max\left(\left|\begin{array}{l} \varepsilon\left(1+\mathrm{B}_{i,j}^{n+1}\right)\frac{\Gamma_{i-1,j}^{n+1}-2\Gamma_{i,j}^{n+1}+\Gamma_{i+1,j}^{n+1}}{\Delta x^2}+\varepsilon\left(1+\mathrm{C}_{i,j}^{n+1}\right)\frac{\Gamma_{i,j-1}^{n+1}-2\Gamma_{i,j}^{n+1}+\Gamma_{i,j+1}^{n+1}}{\Delta y^2} \\ -\left(\frac{\psi_{i,j+1}^{n+1}-\psi_{i,j-1}^{n+1}}{2\Delta y}+\mathrm{D}_{i,j}^{n+1}\right)\frac{\Gamma_{i+1,j}^{n+1}-\Gamma_{i-1,j}^{n+1}}{2\Delta x} \\ +\left(\frac{\psi_{i+1,j}^{n+1}-\psi_{i-1,j}^{n+1}}{2\Delta x}+\mathrm{E}_{i,j}^{n+1}\right)\frac{\Gamma_{i,j+1}^{n+1}-\Gamma_{i,j-1}^{n+1}}{2\Delta y} \\ +\frac{\eta}{\Upsilon_1}\frac{T_{i+1,j}^{n+1}-T_{i-1,j}^{n+1}}{2\Delta x}-F_{i,j}^{n+1} \end{array}\right|\right), \tag{44}$$

$$(\mathrm{Re}\,s_2)_\psi = \max\left(\left|\frac{\psi_{i,j}^{n+1}-\psi_{i,j}^{n}}{\psi_{i,j}^{n+1}}\right|\right), \tag{45}$$

$$(\mathrm{Re}\,s_2)_\Gamma = \max\left(\left|\frac{\Gamma_{i,j}^{n+1}-\Gamma_{i,j}^{n}}{\Gamma_{i,j}^{n+1}}\right|\right). \tag{46}$$

To reach relative accuracies of about $(\mathrm{Re}\,s_2)_\psi = 10^{-10}$ and $(\mathrm{Re}\,s_2)_\Gamma = 10^{-9}$, the following convergence criterion is adopted:

$$\max\left((\mathrm{Re}\,s_1)_\psi, (\mathrm{Re}\,s_1)_\Gamma\right) \leqslant 10^{-6}. \tag{47}$$

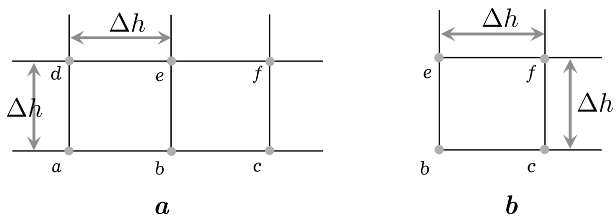

Fig. 2. Generated grid points at the (***a***) wall and the (***b***) corner.

As recommended by Störtkuhl et al. [48], the singularity arising from the vorticity boundary conditions is removed at the corner and wall points by employing the finite element bilinear shape functions, which lead to the following. In this study, we follow Störtkuh et al. for the boundary conditions and use the next approximative expressions:

— At the walls:

$$\frac{1}{3\Delta h^2}\begin{bmatrix} \bullet & \bullet & \bullet \\ 1/2 & -4 & 1/2 \\ 1 & 1 & 1 \end{bmatrix}\psi + \frac{1}{9}\begin{bmatrix} \bullet & \bullet & \bullet \\ 1/2 & 2 & 1/2 \\ 1/4 & 1 & 1/4 \end{bmatrix}\omega = -\frac{V_w}{\Delta h}. \tag{48}$$

— At the corner:

$$\frac{1}{3\Delta h^2}\begin{bmatrix} \bullet & \bullet & \bullet \\ \bullet & -2 & 1/2 \\ \bullet & 1/2 & 1 \end{bmatrix}\psi + \frac{1}{9}\begin{bmatrix} \bullet & \bullet & \bullet \\ \bullet & 1 & 1/2 \\ \bullet & 1/2 & 1/4 \end{bmatrix}\omega = -\frac{V_w}{2\Delta h}. \tag{49}$$

Here, V_w represents the velocity of the considered wall. Based on the above approximations and their schematical illustrations shown in Fig. 2, the nodal vorticity ω_b is computed numerically as:

— At the walls:

$$\omega_b = -\frac{9V_w}{2\Delta h} - \frac{3}{2\Delta h^2}\left(\psi_d+\psi_e+\psi_f\right) - \frac{1}{8}\left(2\omega_a+2\omega_c+\omega_d+4\omega_e+\omega_f\right). \tag{50}$$

— At the corner:

$$\omega_b = -\frac{9V_w}{2\Delta h} - \frac{3}{\Delta h^2}\psi_f - \frac{1}{4}\left(2\omega_c+2\omega_e+\omega_f\right). \tag{51}$$

The local heat transfer rate Nu i.e., local Nusselt number) and its averaged value $\overline{\mathrm{Nu}}$ are scrutinized at the vertical cold wall $x=0$ in the stationary regime as follows:

$$\mathrm{Nu}(y) = -k_r\left(\frac{\partial T}{\partial x}\right)_{x=0}, \tag{52}$$

$$\overline{\mathrm{Nu}} = \int_0^1 \mathrm{Nu}(y)\,dy. \tag{53}$$

4. Results and discussion

Table 2. Comparison between the present numerical results and those of the existing literature in terms of $\overline{\mathrm{Nu}}$ for various values of Ra.

Ra	10^3	10^4	10^5
De Vahl Davis [49]	1.118	2.243	4.519
Barakos et al. [50]	1.114	2.245	4.510
Khanafer et al. [51]	1.118	2.245	4.522
Present results	1.117	2.242	4.922

To prove the exactness of the results exhibited in the present numerical outcomes, the proposed fourth-order compact finite-difference algorithm has been coded in FORTRAN language and then tested multiply with the results reported previously for the natural and mixed convections by De Vahl Davis [49], Barakos et al. [50], Khanafer et al. [51], Khanafer and Chamkha [35] and Waheed [36] as shown in Table 2 and Table 3. As expected, it is found an admissible agreement with the comparing literature works. Indeed, the applied implicit schemes are unconditionally stable and their convergences are assured technically during the computational executions via the residual errors defined by Eqs. (43)–(46).

Table 3. Comparison between the present numerical results and those of the existing literature in terms of $\overline{\mathrm{Nu}}$ for various values of Re_w, when $Gr = 100$.

Re_w	Present results	Khanafer and Chamkha [35]	Waheed [36]
100	2.052	2.01	2.03116
400	4.083	3.91	4.02462
1000	6.599	6.33	6.48423

Table 4. Numerical estimation of the effective values of the average Nusselt number $\overline{\mathrm{Nu}}$ and thermal enhancement E_T for various values of χ, when $\mathrm{Ri} = 8$ and $d_{np} = 30\,\mathrm{nm}$.

χ	$\overline{\mathrm{Nu}}$	$E_T = \frac{\left(\overline{\mathrm{Nu}}_{\chi\neq 0}-\overline{\mathrm{Nu}}_{\chi=0}\right)\times 100}{\overline{\mathrm{Nu}}_{\chi=0}}$
0.00	2.6200	—
0.01	2.6683	1.8435%
0.02	2.6826	2.3893%
0.03	2.6872	2.5648%
0.04	2.6839	2.6450%

After executing properly the established FOCFDM code, several graphical and tabular results have been outputted numerically in Figs. 3–12 and Table 4 for streamlines $\psi(x,y)$, isotherms $T(x,y)$, longitudinal velocity fields $U(x=0.5,y)$, horizontal temperature distributions $T(x,y=0.5)$, and local Nusselt number profiles Nu. Those illustrations are done correspondingly for sundry values of the embedded physical parameters, namely mixed convection parameter (i.e., Richardson number) Ri, nanoparticles volume fraction χ, and nanoparticles diameter size d_{np}, with default values being selected appropriately $\mathrm{Ri} = 8$, $\chi = 0.01$, and $d_{np} = 30\,\mathrm{nm}$. For revealing the characteristic of the present dynamical system and its heat transfer feature towards the increasing values of the mixed convection parameter Ri, various streamlines and isotherms are shown in Fig. 3 for water H_2O and copper-water nanofluid Cu-H_2O. From the graphical illustrations of Fig. 3 (left), it is evident that the mixed convection flow is characterized by a strong circulation motion in the middle of the cavity with the appearance of counterclockwise rotating main cells. Also, it is perceived the development of two clockwise secondary cells from either vertical side of the cavity, which are centrally symmetrical spatially. Further, the deformed isotherms depicted in Fig. 3 (right) prove that the heat transfer communicated by the mixed convection heat transfer mechanism is more important near the lower corner of the vertical cold wall $x = 0$ because of the higher value of the temperature gradient. Due to the domination of the natural convection over the forced convection, the mixed convection parameter Ri is intensified numerically, which leads to a slight change in the flow pattern as seen in Fig. 3 (left). As the main results of this augmentation, the magnitude of the longitudinal velocity $U(x=0.5,y)$ along the vertical mid-plane $x = 0.5$ is improved remarkably as elucidated in Fig. 4 and the horizontal temperature $T(x,y=0.5)$ throughout the mid-plane $y = 0.5$ is enhanced near the cold wall $x = 0$ and diminished near the hot wall $x = 1$ as emphasized in Fig. 5. Further, the distribution of heat transfer rate through the cold wall $x = 0$ is estimated locally for different values of the mixed convection parameter Ri as displayed in Fig. 6. From this graphical demonstration, it is noticed a significant upsurge in the local heat transfer rate $\mathrm{Nu}(y)$ near the upper corner of the cold wall $x = 0$

as long as the physical parameter Ri is strengthened. However, a reverse trend is witnessed far from the upper corner of the cold wall $x = 0$.

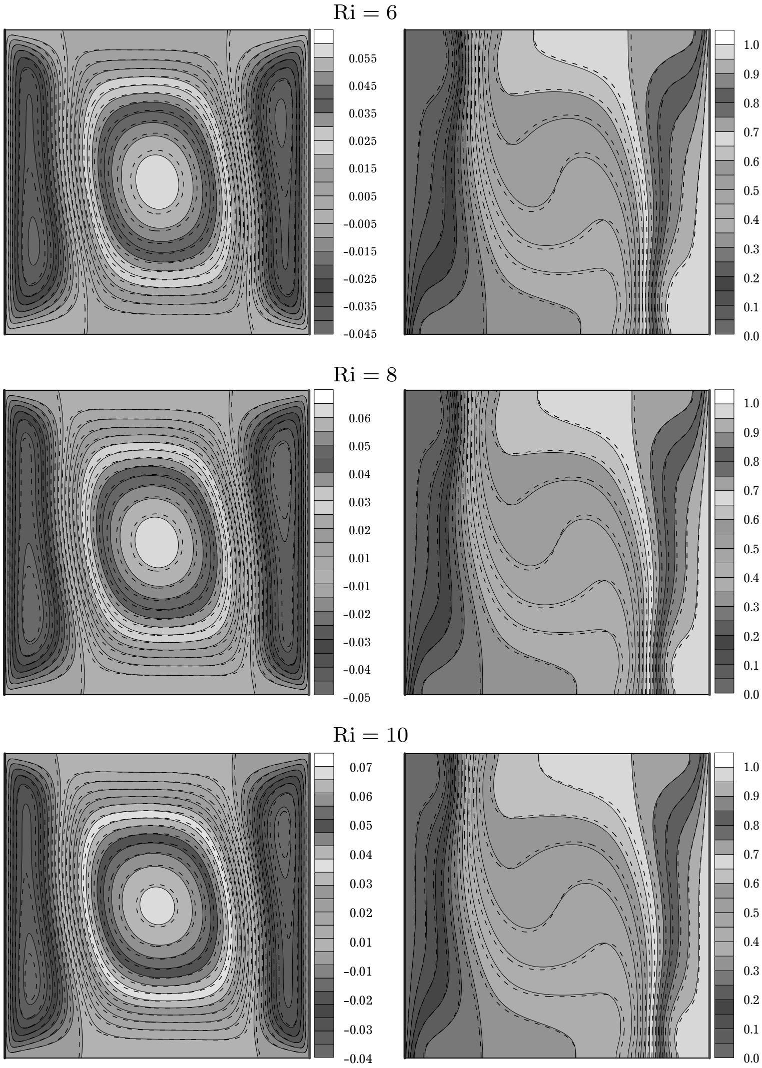

Fig. 3. Streamline shapes (left) and isotherm contours (right) of water (dashed line) and copper-water nanofluid (solid line) for various values of Ri, when $\chi = 0.01$ and $d_{np} = 30\,\text{nm}$.

Fundamentally, the nanoparticles loading causes an increase in the effective value of the dynamic viscosity of the nanofluidic medium. For this reason, the magnitude of the longitudinal velocity $U(x = 0.5, y)$ shows a declining trend along the vertical mid-plane $x = 0.5$ in Fig. 7, when the nanoparticles volume fraction χ is increased. A dual behavior is perceived in Fig. 8 for the profiles of the horizontal temperature $T(x, y = 0.5)$ throughout the mid-plane $y = 0.5$, which is dwindled near the cold wall $x = 0$ and amplified near the hot wall $x = 1$. As a result of this nonlinear thermal distribution, an enhancement in the local heat transfer rate $\mathrm{Nu}(y)$ is remarked near the upper corner of the cold wall $x = 0$ with the higher estimate values of the nanoparticles volume fraction χ as ascertained in Fig. 9. Whilst, an opposite variation is witnessed near the lower corner of the cold wall $x = 0$. Despite this contrast, the results of Table 4 confirm that the averaged heat transfer rate $\overline{\mathrm{Nu}}$ and its corresponding thermal enhancement E_T are increasing functions of the nanoparticles volume fraction χ. From a physical standpoint, an increase in the nanoparticles diameter size d_{np} improves somewhat the fluidity feature of the homogeneous nanofluidic medium and leads to a quiet escalation in the magnitude of the longitudinal velocity $U(x = 0.5, y)$ along the vertical mid-plane $x = 0.5$ as disclosed in Fig. 10. The reason behind this fact is that the nanofluid viscosity $\mu_{nf} = \mu_f\left[1 - 34.87(d_{np}/d_f)^{-0.3}\chi^{1.03}\right]^{-1}$ is a decreasing function of the dimensional parameter d_{np}. Other thermal feature id explored in Fig. 11

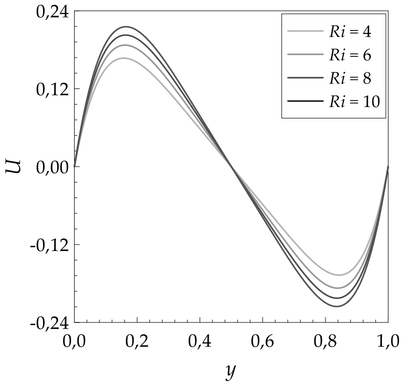

Fig. 4. Longitudinal velocity profiles along the mid-plane $x = 0.5$ for various values of Ri, when $\chi = 0.01$ and $d_{np} = 30\,\text{nm}$.

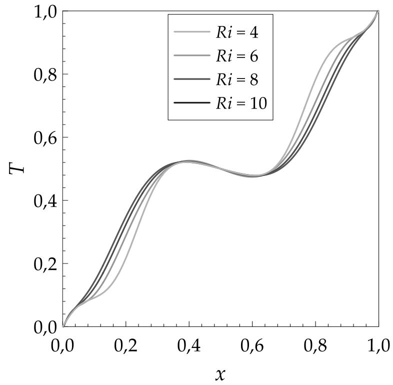

Fig. 5. Horizontal temperature profiles along the mid-plane $y = 0.5$ for various values of Ri, when $\chi = 0.01$ and $d_{np} = 30\,\text{nm}$.

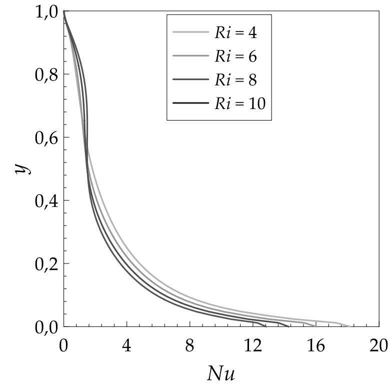

Fig. 6. Local Nusselt number profiles at the vertical cold wall $x = 0$ for various values of Ri, when $\chi = 0.01$ and $d_{np} = 30\,\text{nm}$.

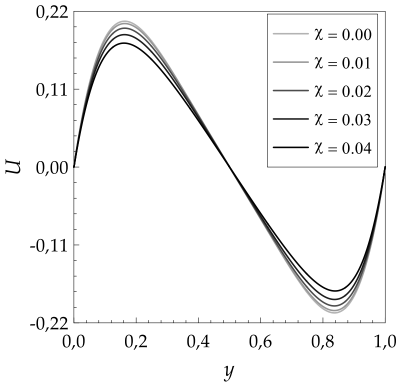

Fig. 7. Longitudinal velocity profiles along the mid-plane $x = 0.5$ for various values of Ri, when $\chi = 0.01$ and $d_{np} = 30\,\text{nm}$.

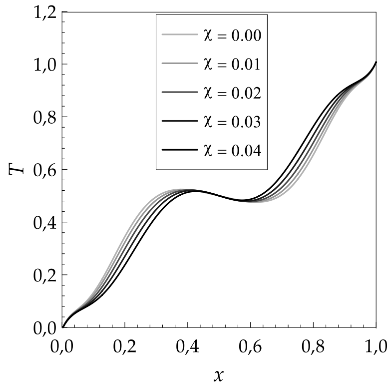

Fig. 8. Horizontal temperature profiles along the mid-plane $y = 0.5$ for various values of χ, when $\text{Ri} = 8$ and $d_{np} = 30\,\text{nm}$.

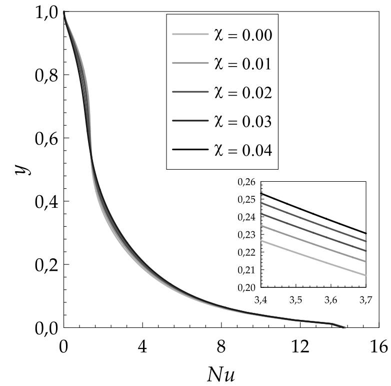

Fig. 9. Local Nusselt number profiles at the vertical cold wall $x = 0$ for various values of χ, when $\text{Ri} = 8$ and $d_{np} = 30\,\text{nm}$.

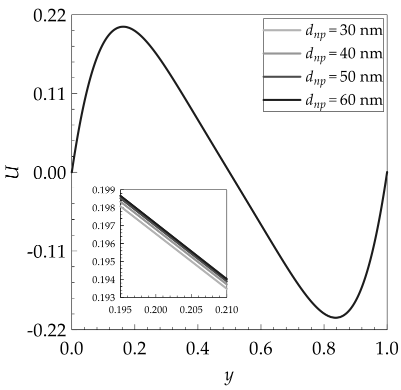

Fig. 10. Longitudinal velocity profiles along the mid-plane $x = 0.5$ for various values of d_{np}, when $\text{Ri} = 8$ and $\chi = 0.01$.

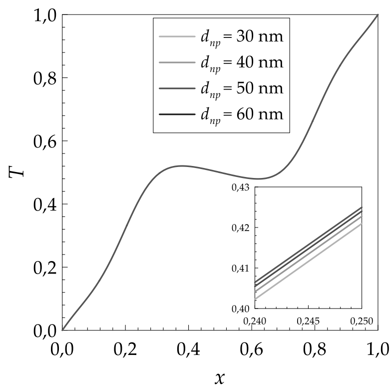

Fig. 11. Horizontal temperature profiles along the mid-plane $x = 0.5$ for various values of d_{np}, when $\text{Ri} = 8$ and $\chi = 0.01$.

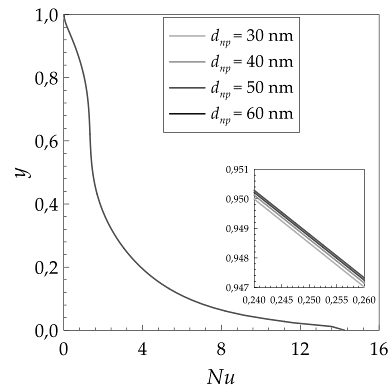

Fig. 12. Local Nusselt number profiles at the vertical cold wall $x = 0$ for various values of d_{np}, when $\text{Ri} = 8$ and $\chi = 0.01$.

concerning the effect of the nanoparticles diameter size d_{np} on the distribution of the temperature $T(x, y = 0.5)$ throughout the horizontal mid-plane $y = 0.5$. From this graphical representation, it is obvious that the geometrical parameter d_{np} has a slight enhancing thermal impact on the nanofluidic medium. This fact is explained by the enlargement in the surface exchange between the solid nanoparticles and the surrounding base fluid, which in turn improves some bits the local heat transfer rate at the cold wall $x = 0.5$ as clarified in Fig. 12.

5. Conclusion

The main concluding remarks are itemized as follows:

— The proposed FOCFDM numerical algorithm shows a flexible capability in solving a complex differential system of coupled partial differential equations (PDEs), which is too complicated to be solved analytically or semi-analytically for a two-dimensional geometrical convective flow.
— The present FOCFDM outcomes are validated multiply with those reported previously by pioneering researchers.
— The longitudinal motion of the nanofluid is boosted either by the increase in both the mixed convection parameter Ri and the nanoparticles diameter size d_{np}. However, the nanoparticles volume fraction χ exhibits a postponing impact of the nanofluid motion.
— The mixed convection parameter Ri and the nanoparticles volume fraction χ show a dual behavior against the temperature distribution.
— The nanoparticles loading and the higher values of the nanoparticles diameter size d_{np} enhance the heat transfer rate at the cold wall.

[1] Aly A. M., Raizah Z. A. S., Sheikholeslami M. Analysis of mixed convection in a sloshing porous cavity filled with a nanofluid using ISPH method. Journal of Thermal Analysis and Calorimetry. **139**, 1977–1991 (2020).

[2] Muhammad N., Nadeem S., Issakhov A. Finite volume method for mixed convection flow of Ag-ethylene glycol nanofluid flow in a cavity having thin central heater. Physica A: Statistical Mechanics and its Applications. **537**, 122738 (2020).

[3] Jamesahar E., Sabour M., Shahabadi M., Mehryan S. A. M., Ghalambaz M. Mixed convection heat transfer by nanofluids in a cavity with two oscillating flexible fins: A fluid-structure interaction approach. Applied Mathematical Modelling. **82**, 72–90 (2020).

[4] Alsabery A. I., Armaghani T., Chamkha A. J., Hashim I. Two-phase nanofluid model and magnetic field effects on mixed convection in a lid-driven cavity containing heated triangular wall. Alexandria Engineering Journal. **59**, 129–148 (2020).

[5] Qasim M., Ali Z., Wakif A., Boulahia Z. Numerical simulation of MHD peristaltic flow with variable electrical conductivity and Joule dissipation using generalized differential quadrature method. Communications in Theoretical Physics. **71**, 509–518 (2019).

[6] Afridi I. M., Qasim M., Wakif A., Hussanan A. Second Law Analysis of Dissipative Nanofluid Flow over a Curved Surface in the Presence of Lorentz Force: Utilization of the Chebyshev–Gauss–Lobatto Spectral Method. Nanomaterials. **9** (2), 195 (2019).

[7] Amanulla C. H., Wakif A., Boulahia Z., Fazuruddin S., Mohammed S. N. A Study on Non-Newtonian Transport Phenomena in MHD Fluid Flow From a Vertical Cone With Navier Slip and Convective Heating. Nonlinear Engineering. **8** (1), 534–545 (2019).

[8] Qasim M., Afridi M. I., Wakif A., Saleem S. Influence of Variable Transport Properties on Nonlinear Radioactive Jeffrey Fluid Flow Over a Disk: Utilization of Generalized Differential Quadrature Method. Arabian Journal for Science and Engineering. **44**, 5987–5996 (2019).

[9] Qasim M., Afridi M. I., Wakif A., Thoi T. N., Hussanan A. Second Law Analysis of Unsteady MHD Viscous Flow over a Horizontal Stretching Sheet Heated Non-Uniformly in the Presence of Ohmic Heating: Utilization of Gear-Generalized Differential Quadrature Method. Entropy. **21** (3), 240 (2019).

[10] Amanulla C. H., Saleem S., Wakif A., AlQarni M. M. MHD Prandtl fluid flow past an isothermal permeable sphere with slip effects. Case Studies in Thermal Engineering. **14**, 100447 (2019).

[11] Wakif A., Qasim M., Afridi M. I., Saleem S., Al-Qarni M. M. Numerical Examination of the Entropic Energy Harvesting in a Magnetohydrodynamic Dissipative Flow of Stokes' Second Problem: Utilization of the Gear-Generalized Differential Quadrature Method. Journal of Non-Equilibrium Thermodynamics. **44** (4), 385–403 (2019).

[12] Wakif A. A novel numerical procedure for simulating steady MHD convective flows of radiative Casson fluids over a horizontal stretching sheet with irregular geometry under the combined influence of temperature-dependent viscosity and thermal conductivity. Math. Probl. Eng. **2020**, Article ID: 1675350 (2020).

[13] Diouf M., Sene N. Analysis of the financial chaotic model with the fractional derivative operator. Complexity. **2020**, Article ID: 9845031 (2020).

[14] Sene N. Second-grade fluid model with Caputo-Liouville generalized fractional derivative. Chaos, Solitons & Fractals. **133**, 109631 (2020).

[15] Haq R. U., Usman M., Algehyne E. A. Natural convection of CuO-water nanofluid filled in a partially heated corrugated cavity: KKL model approach. Communications in Theoretical Physics. **72**, 85003 (2020).

[16] Seyyedi S. M., Dogonchi A. S., Hashemi-Tilehnoee M., Waqas M., Ganji D. D. Investigation of entropy generation in a square inclined cavity using control volume finite element method with aided quadratic Lagrange interpolation functions. International Communications in Heat and Mass Transfer. **110**, 104398 (2020).

[17] Syrakos A., Dimakopoulos Y., Tsamopoulos J. A finite volume method for the simulation of elastoviscoplastic flows and its application to the lid-driven cavity case. Journal of Non-Newtonian Fluid Mechanics. **275**, 104216 (2020).

[18] Sajjadi H., Mohammadifar H., Amiri Delouei A. Investigation of the effect of the internal heating system position on heat transfer rate utilizing Cu/water nanofluid. Journal of Thermal Analysis and Calorimetry. **139**, 2035–2054 (2020).

[19] Buongiorno J. et al. A benchmark study on the thermal conductivity of nanofluids. Journal of Applied Physics. **106**, 094312 (2009).

[20] Nayak M. K. Wakif A., Animasaun I. L., Alaoui M. S. H. Numerical Differential Quadrature Examination of Steady Mixed Convection Nanofluid Flows Over an Isothermal Thin Needle Conveying Metallic and Metallic Oxide Nanomaterials: A Comparative Investigation. Arabian Journal for Science and Engineering. **45**, 5331–5346 (2020).

[21] Tiwari R. K., Das M. K. Heat transfer augmentation in a two-sided lid-driven differentially heated square cavity utilizing nanofluids. International Journal of Heat and Mass Transfer. **50** (9–10), 2002–2018 (2007).

[22] Eid M. R., Mahny K. L., Dar A., Muhammad T. Numerical study for Carreau nanofluid flow over a convectively heated nonlinear stretching surface with chemically reactive species. Physica A: Statistical Mechanics and its Applications. **540**, 123063 (2020).

[23] Rasool G., Chamkha A. J., Muhammad T., Shafiq A., Khan I. Darcy–Forchheimer relation in Casson type MHD nanofluid flow over non-linear stretching surface. Propulsion and Power Research. **9** (2), 159–168 (2020).

[24] Ahmad M., Muhammad T., Ahmad I., Aly S. Time-dependent 3D flow of viscoelastic nanofluid over an unsteady stretching surface. Physica A: Statistical Mechanics and its Applications. **551**, 124004 (2020).

[25] Hayat T., Haider F., Muhammad T., Alsaedi A. Darcy–Forchheimer flow of carbon nanotubes subject to heat flux boundary condition. Physica A: Statistical Mechanics and its Applications. **554**, 124002 (2020).

[26] Naqvi S. M. R. S., Muhammad T., Saleem S., Kim H. M. Significance of non-uniform heat generation/absorption in hydromagnetic flow of nanofluid due to stretching/shrinking disk. Physica A: Statistical Mechanics and its Applications. **553**, 123970 (2020).

[27] Rana P., Bhargava R. Numerical study of heat transfer enhancement in mixed convection flow along a vertical plate with heat source/sink utilizing nanofluids. Communications in Nonlinear Science and Numerical Simulation. **16** (11), 4318–4334 (2011).

[28] Zaraki A., Ghalambaz M., Chamkha A. J., Ghalambaz M., De Rossi D. Theoretical analysis of natural convection boundary layer heat and mass transfer of nanofluids: Effects of size, shape and type of nanoparticles, type of base fluid and working temperature. Advanced Powder Technology. **26** (3), 935–946 (2015).

[29] Buongiorno J. Convective Transport in Nanofluids. Journal Heat Transfer. **128** (3), 240–250 (2006).

[30] Mebarek-Oudina F. Convective heat transfer of Titania nanofluids of different base fluids in cylindrical annulus with discrete heat source. Heat Transfer-Asian Res. **48**, 135–147 (2019).

[31] Wakif A., Boulahia Z., Sehaqui R. Numerical analysis of the onset of longitudinal convective rolls in a porous medium saturated by an electrically conducting nanofluid in the presence of an external magnetic field. Results in Physics. **7**, 2134–2152 (2017).

[32] Wakif A., Boulahia Z., Sehaqui R. A Semi-Analytical Analysis of Electro-Thermo-Hydrodynamic Stability in Dielectric Nanofluids Using Buongiorno's Mathematical Model Together with More Realistic Boundary Conditions. Results in Physics. **9**, 1438–1454 (2018).

[33] Wakif A., Boulahia Z., Mishra S. R., Mehdi Rashidi M., Sehaqui R. Influence of a uniform transverse magnetic field on the thermo-hydrodynamic stability in water-based nanofluids with metallic nanoparticles using the generalized Buongiorno's mathematical model. The European Physical Journal Plus. **133**, Article number: 181 (2018).

[34] Wakif A., Animasaun I. L., Satya Narayana P. V., Sarojamma G. Meta-analysis on thermo-migration of tiny/nano-sized particles in the motion of various fluids. Chinese Journal of Physics. **68**, 293–307 (2020).

[35] Khanafer K. M., Chamkha A. J. Mixed convection flow in a lid-driven enclosure filled with a fluid-saturated porous medium. International Journal of Heat and Mass Transfer. **42** (13), 2465–2481 (1999).

[36] Waheed M. A. Mixed convective heat transfer in rectangular enclosures driven by a continuously moving horizontal plate. International Journal of Heat and Mass Transfer. **52** (21–22), 5055–5063 (2009).

[37] Ghaffari A., Mustafa I., Javed T. Influence of nonlinear radiation on natural convection flow of carbon nanotubes suspended in water-based fluid along a vertical wavy surface. Physica Scripta. **94**, 115214 (2019).

[38] Mustafa I., Ghaffari A., Javed T., Abbasi J. N. Numerical Examination of Thermophysical Properties of Cobalt Ferroparticles over a Wavy Surface Saturated in Non-Darcian Porous Medium. J. Non-Equilibrium Thermodyn. **45** (2), 109–120 (2020).

[39] Wakif A., Boulahia Z., Amine A., Animasaun I. L., Afridi M. I., Qasim M., Sehaqui R. Magneto-convection of alumina - water nanofluid within thin horizontal layers using the revised generalized Buongiorno's model. Frontiers in Heat and Mass Transfer. **12**, 3 (2019).

[40] Wakif A., Chamkha A., Thumma T., Animasaun I. L., Sehaqui R. Thermal radiation and surface roughness effects on the thermo-magneto-hydrodynamic stability of alumina-copper oxide hybrid nanofluids utilizing the generalized Buongiorno's nanofluid model. Journal of Thermal Analysis and Calorimetry. **143**, 1201–1220 (2020).

[41] Corcione M. Empirical Correlating Equations for Predicting the Effective Thermal Conductivity and Dynamic Viscosity of Nanofluids. Energy Conversion and Management. **52** (1), 789–793 (2011).

[42] Shah N. A., Animasaun I. L., Wakif A., Koriko O. K., Sivaraj R., Adegbie K. S., Abdelmalek Z., Vaidyaa H., Ijirimoye A. F., Prasad K. V. Significance of suction and dual stretching on the dynamics of various hybrid nanofluids: Comparative analysis between type I and type II models. Physica Scripta. **95** (9), 95205 (2020).

[43] Iqbal M. S., Mustafa I., Riaz I., Ghaffari A., Khan W. A. Influence of carbon nanotubes on heat transfer in MHD nanofluid flow over a stretchable rotating disk: A numerical study. Heat Transfer. **50**, 619–637 (2020).

[44] Wakif A., Boulahia Z., Ali F., Eid M. R., Sehaqui R. Numerical Analysis of the Unsteady Natural Convection MHD Couette Nanofluid Flow in the Presence of Thermal Radiation Using Single and Two-Phase Nanofluid Models for Cu-Water Nanofluids. International Journal of Applied and Computational Mathematics. **4**, Article number: 81 (2018).

[45] Erturk E. Numerical performance of compact fourth-order formulation of the Navier–Stokes equations. Communications in Numerical Methods in Engineering. **24**, 2003–2019 (2008).

[46] Peaceman D. W., Rachford J. H. H. The Numerical Solution of Parabolic and Elliptic Differential Equations. Journal of the Society for Industrial and Applied Mathematics. **3** (1), 28–41 (1955).

[47] Erturk E., Gökcötol C. Fourth-order compact formulation of Navier–Stokes equations and driven cavity flow at high Reynolds numbers. International Journal for Numerical Methods in Fluids. **50** (4), 421–436 (2006).

[48] Störtkuhl T., Zenger C., Zimmer S. An asymptotic solution for the singularity at the angular point of the lid driven cavity. International Journal of Numerical Methods for Heat & Fluid Flow. **4** (1), 47–59 (1994).

[49] De Vahl Davis G. Natural convection of air in a square cavity: A benchmark numerical solution. International Journal for Numerical Methods in Fluids. **3**, 249–264 (1983).

[50] Barakos G., Mitsoulis E., Assimacopoulos D. Natural convection flow in a square cavity revisited: Laminar and turbulent models with wall functions. International Journal for Numerical Methods in Fluids. **18**, 695–719 (1994).

[51] Khanafer K., Vafai K., Lightstone M. Buoyancy-driven heat transfer enhancement in a two-dimensional enclosure utilizing nanofluids. International Journal of Heat and Mass Transfer. **46** (19), 3639–3653 (2003).

Чисельне дослідження характеристик змішаної конвекційної теплопередачі в мідно-водному нанофлюїдному середовищі, що займає квадратну геометричну порожнину

Зайдан М., Вакіф А., Ессагір Е., Сехакі Р.

Лабораторія механіки, Факультет наук Ан-Чок,
Університет Хасана II Касабланка, Марокко

В представленій роботі явище змішаної конвекційно-теплової передачі в однорідних сумішах ретельно досліджується для випадку мідно-водяної нанорідини, що протікає усередині квадратної порожнини. Застосовуючи наближення Обербека–Буссінеска та використовуючи однофазну нанорідку модель, диференціальні рівняння зі частинними похідними, що моделюють реальний потік, сформульовані математично на основі теорії Нав'є–Стокса та теплового балансу, де важливі особливості досліджуваного середовища вважаються постійними при низьких температурах. Зазначимо, що величина густини в об'ємній силі плавучості тіла є лінійною функцією, залежною від температури. Характерні величини реалістично обчислюються за допомогою загальновживаних феноменологічних законів та більш точних експериментальних кореляцій. Для виведення безрозмірних рівнянь збереження застосовано процедуру знерозмірення. Отримані нелінійні диференціальні рівняння розв'язано чисельно для реалістичних граничних умов за допомогою компактного скінченно-різницевого методу четвертого порядку (КСРМЧП). Після проведення значних перевірок з опублікованими раніше результатами, з'ясовано, що динамічні та теплові характеристики, отримані для досліджуваного конвективного потоку нанорідини добре узгоджуються для різних значень задіяних фізичних параметрів. Крім того, представлені чисельні результати обговорені графічно та таблично за допомогою потокових ліній, ізотерм, полів швидкості, розподілу температури та локальних профілів теплопередачі.

Ключові слова: *нанорідина, змішана конвекція, квадратна порожнина, чисельне моделювання.*